Proceedings of the ASME 2010 3rd Joint US-European Fluids Engineering Summer Meeting and 8th International Conference on Nanochannels, Microchannels, and Minichannels
FEDSM-ICNMM2010
August 1-5, 2010, Montreal, Canada

FEDSM-ICNMM2010-30515

ACTIVE CONTROL OF VORTEX INDUCED VIBRATION BY PLASMA ACTUATION

Sari Gh.

Department of Electrical Engineering,
École Polytechnique, Montréal,
Que., H3T 1J4, CANADA

Mureithi N.W.

BWC/AECL/NSERC Chair of Fluid-Structure Interaction
Department of Mechanical Engineering,
École Polytechnique, Montréal,
Que., H3T 1J4, CANADA

Nomenclature

VIV: Vortex Induced Vibration
SDBD: Single Dielectric Barrier Discharge
FIM: Fisher Information Matrix
HC: Hartlen-Currie
DAQ: Data Acquisition
SMC: Sliding Mode Control
PIV: Particle Image Velocimetry
C_l: Lift coefficient
ω_0: Ratio of the Strouhal shedding frequency to the natural frequency of the cylinder
τ: Non-dimensional time
x_r : Dimensionless cylinder displacement
ζ : Material damping factor
f_n : Natural frequency of cylinder

ABSTRACT

In this paper, the results of experiments on the elimination of vortex induced vibration (VIV) of a cylinder in cross-flow by using a simple active control method are reported. Motivated by new research, a Single Dielectric Barrier Discharge (SDBD) plasma actuator is used and the effect of steady and unsteady actuation demonstrated. The feasibility of the model parameters estimation was also studied in simulations by investigating the Fisher Information Matrix and the nonlinear numerical curve fitting methods applied to estimate identifiable parameters from experimental data. The efficiency of the control methods was found to be acceptable and simulation outcomes supported the experimental results.

1 INTRODUCTION

Vortex-induced vibration is an important problem in many fields of engineering. It may cause noise, affect the fatigue life of structures and even result in structural damage. Understanding and controlling VIV has therefore attracted significant attention. Research on VIV has led to the design and developments of active methods that eliminate the periodic force caused by vortex shedding and lessen or completely suppress the vibrations. In studies of vortex-induced vibration, the case of an elastically mounted circular cylinder, constrained to move transverse to an oncoming flow, is often used as a paradigm. In this paper, we have employed this traditional model to develop an active control approach focused on vibration control.

In order to suppress both vortex shedding and structural vibration, various active control methods have been explored in the past. Acoustic excitation [1–2] and cylinder rotation [3] are recognized as precursory methods for active flow control. Cheng et al. [4] introduced a novel perturbation technique using embedded piezoelectric actuators for elastically mounted cylinders, which was found to efficiently alter the interaction between the flow and the structure vibration.

In this work the vibration was eliminated by plasma actuation because of considerable interests in using of electric discharge plasma for flow control in recent years and experimental investigations showing its dramatic effect on the gas flow [10]. DBD plasma actuators are known to be effective in aerodynamic control [19-20]. They produce a body force on the air by an electric field acting on the ions in the vicinity of the actuator electrode, providing the potential for flow control [9].

A particular problem with the plasma actuator is power consumption. Unsteady actuation is an easy solution to this problem. Motivated by this we investigate the effect of unsteady actuation on the generated force and vibration control.

The wake-oscillator model proposed by Hartlen-Currie [5] was used to develop the control approaches. The oscillator is self-exciting and self-limiting and with the appropriate choice of parameters, the model qualitatively captures many of the features seen in experimental results. In order to estimate the parameters by experimental data, we focused at first on investigating the systematic parameter identifiability based on a study of the Fisher Information Matrix (FIM). The FIM quantifies the amount of information that an observable random variable carries about an unknown parameter.

Finally a sliding mode controller was designed to suppress the vortex induced vibration. Sliding mode control is known to be an effective robust control technique applicable to a wide class of nonlinear systems as well as vortex induced vibration of an elastically mounted circular cylinder which are subject to modeling uncertainty and external disturbances [13,14]. This control method is of particular interest in simulation and in practice, among them relative simplicity of design and invariance to parameter and external perturbations.

The main contributions of this work are:

(1) Demonstration of the limits of identifiability of parameters in the Hartlen-Currie model from measured response data.
(2) Development and demonstration of a simple and robust relay sliding mode controller employing plasma actuators for VIV control.

2 MATERIALS AND METHODS

2.1 Wake Oscillator Model

Hartlen and Currie [5] formulated a semi-empirical oscillator model to represent the large amplitude oscillations which occur when the vortex-shedding frequency is near the natural frequency of the cylinder. In their model, a van der Pol nonlinear oscillator for the lift force is coupled to the cylinder motion by a linear dependence on the cylinder velocity. The cylinder displacement is perpendicular to both cylinder axis and the flow direction. The resulting equations are:

$$x_r'' + 2\zeta x_r' + x_r = a\omega_0^2 C_l \quad (1)$$

$$C_l'' - \alpha\omega_0 C_l' + \frac{\gamma}{\omega_0}(C_l')^3 + \omega_0^2 C_l = b x_r' \quad (2)$$

where the time derivative is with respect to the non-dimensional time $\boldsymbol{\tau = \omega_n t}$, $\boldsymbol{x_r}$ is the dimensionless cylinder displacement, $\boldsymbol{C_l}$ is the lift coefficient, $\boldsymbol{\omega_0}$ is the ratio of the Strouhal shedding frequency to the natural frequency of the cylinder, $\boldsymbol{\omega_0 = f_0/f_n}$, and $\boldsymbol{\zeta}$ is the material damping factor. The parameter $\boldsymbol{a}$ is a known dimensionless constant. The three remaining parameters, $\boldsymbol{\alpha}$, $\boldsymbol{\gamma}$ and $\boldsymbol{b}$ must be chosen to provide the best fit to experimental data and parameters $\boldsymbol{\alpha}$ and $\boldsymbol{\gamma}$ are related to each other by the expression $\boldsymbol{C_{l_0} = (\frac{4\alpha}{3\gamma})^{1/2}}$; where $\boldsymbol{C_{l_0}}$ is the amplitude of the fluctuation of $\boldsymbol{C_l}$ on a fixed cylinder.

The oscillator is self-exciting and self-limiting; the second term on the left-hand side of Eq. (2) provides the growth of the lift coefficient $\boldsymbol{C_l}$, while the third term on the left-hand side of the same equation prevents its unlimited growth. If the parameters are selected appropriately a large amplitude vibration can be obtained when the vortex shedding frequency is near the natural frequency of the cylinder and in this condition the vibration frequency remains almost constant. This peak value of oscillation and the hysteresis effect seen in the experimental results has also be observed in the bifurcation analysis of the HC model by Mureithi al. [6,7].

2.2 Investigation of Parameter Identifiability by FIM

An important problem, associated with VIV models is the estimation of the model parameters from experimental data. The process of parameter identification is an inverse problem which can be ill conditioned. The aim of this section is to investigate the identifiability of parameters for the HC model. The parameters will be later estimated by using the results obtained from dynamical tests.

Systematic identifiability analysis is based on the Fisher Information Matrix (FIM). The analysis depends on the available information such as the observed components, and the measurement precision. The impact of the experimental conditions is unknown in advance but can be evaluated via the FIM. The structure of the HC model enables us to compute the FIM as precisely as needed. Based on the FIM we can investigate the practical identifiability of parameters in the model, i.e., the accuracy of the estimation that can be hoped for by measuring the displacement. It is worth noting that in this work we can only measure the displacement of the cylinder.

In the HC model the FIM reveals the amount of information that the cylinder displacement $\boldsymbol{x_r}$ carries about each of the unknown parameters $\boldsymbol{\theta}$ upon which the likelihood function of $\boldsymbol{\Theta}$, $\mathbf{L(\Theta)}$, depends. Hence the FIM is given by:

$$\mathrm{FIM}(\Theta) = \mathrm{E}\left\{\left[\frac{\partial}{\partial\Theta}\ln\left(\mathrm{L}(\Theta)\right)\right]^2 |\Theta\right\} \quad (3)$$

$$\mathrm{L}(\Theta) = \mathrm{f}(\mathrm{x_r}, \Theta) \quad (4)$$

There are 5 parameters in the HC model, so θ is a 5x1 vector $\boldsymbol{\Theta = [\zeta, a, b, \gamma, \alpha]}$ and the FIM takes the form of a 5x5 positive semi-definite symmetric matrix.

We can numerically simulate the model to produce the FIM and then we can estimate the covariance matrix of the parameters.

This matrix can show the accuracy of the parameter estimation that can be hoped for, in the model by measuring the specified variable. Once the variance-covariance matrix is known the variance of any parameter can be obtained from the diagonal elements of the matrix.

$$\begin{bmatrix} \mathrm{Var}(\theta_1) & \dots & \mathrm{Cov}(\theta_1,\theta_5) \\ \vdots & \ddots & \vdots \\ \mathrm{Cov}(\theta_1,\theta_5) & \dots & \mathrm{Var}(\theta_5) \end{bmatrix} = (\mathrm{FIM})^{-1} \quad (5)$$

The FIM is numerically given by

$$\mathrm{FIM} = \Psi' \cdot \Psi_{\ 5\times5} \quad (6)$$

where Ψ is the derivative matrix for each parameter and can be formed by the following algorithm:

(I) Choose the default value of parameters $\zeta = 0.0015,\ \alpha = 0.02, \gamma = 2/3,\ a = 0.002$ and $b = 0.4$ proposed in [5].
(II) Numerically integrate the equations (1) and (2) for a long time interval until the transients are damped out and the remaining steady-state motion is periodic.
(III) Divide the response of the system into equal intervals (e.g. 101) and the variable (here the displacement of the cylinder) measured for each interval. So in this step we will have an array whose dimension is 101.
(IV) Change only one of the parameters by 5% and repeat steps (II) and (III).
(V) Repeat step (IV) for all of the parameters.
(VI) Calculate the derivative matrix in which the columns are Δ(variable)/Δ(parameter). So in this step we have a $\Psi_{\ 101\times5}$ matrix as the derivative matrix.
(VII) Compute $\mathrm{FIM} = (\Psi' \cdot \Psi)_{\ 5\times5}$
(VIII) Covariance Matrix $= \mathrm{FIM}^{-1}$

In the HC model, we will show that the measurement of the displacement is not sufficient to achieve identifiability of all the parameters involved.

2.3 Plasma Actuator

A plasma actuator consists of two electrodes that are separated by a dielectric material. Figure 1 shows a schematic of a linear SDBD plasma actuator. When a sufficiently high ac voltage is supplied to the electrodes, the air above the exposed electrode is ionized. The generated plasma then accelerates the flow toward the embedded electrode. The plasma discharge has a self-limiting character and gives rise to a body force on the ambient air. The body force vector is given by: [8]

$$\vec{\mathrm{f}}_{\mathrm{b}} = \rho_{\mathrm{c}}\vec{\mathrm{E}} \quad (7)$$

Where $\vec{\mathrm{E}}$ is electrical field vector and ρ_c is the charge density.

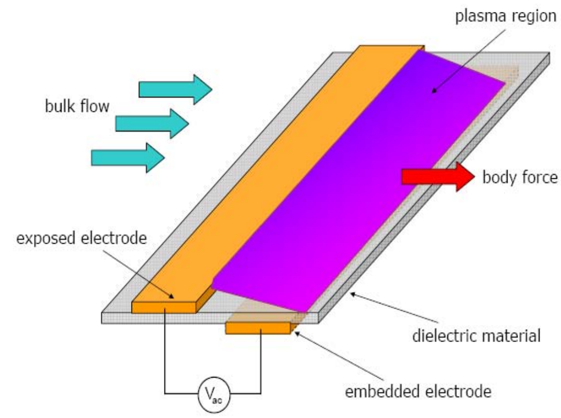

Figure 1- Schematic of SDBD plasma actuator [9]

The electric potential distribution in the vicinity of the electrodes computed by Suzen et al. [9] is shown in Figure 2 along with the streamlines of the actuator induced flow. The streamlines show that the flow will be dragged from above toward the area between the two electrodes and then accelerated to the right. So it is obvious that in the case of appropriately mounted plasma actuators on the surface of the cylinder, the actuation can affect the flow separation and lead directly to vortex shedding perturbation and hence vibration damping. Thomas et al. [10] showed that a set of four plasma actuators mounted on the surface of a pivoted cylinder on the downstream surface can suppress the flow separation effectively.

The results of Roth et al.'s research [11] proved that maximization of the transferred momentum to the neutral gas (air) and induced flow velocity can be accomplished by altering the dielectric material properties, the level of supplied ac voltage, the frequency of the voltage, and the geometrical parameters of the actuator. More importantly, the results showed that the actuation force is not a continuous function of the supplied voltage and frequency. Plasma is initiated after a threshold voltage and the minimum force is not zero at the threshold value. The generated body force is zero at voltages below the threshold value since there is no dielectric barrier discharge. This phenomenon will limit the usage of anti-chattering Sliding Mode Control (SMC) algorithms which will be discussed later. Furthermore, in this work we were only able to change the supplied voltage frequency because of some practical limitations so continuously changing the body force from zero was theoretically and practically impossible.

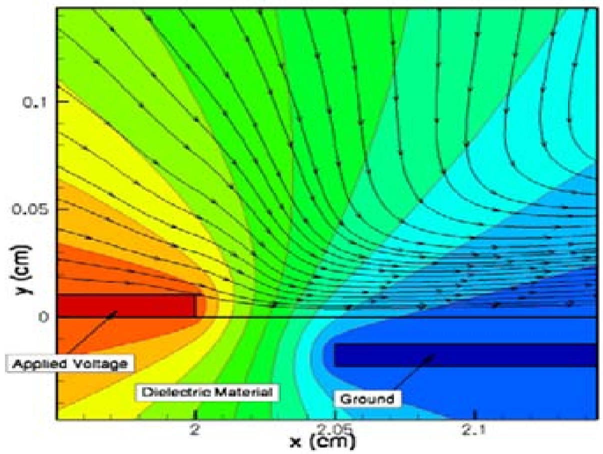

Figure 2- Computed electric potential contours and streamlines in the vicinity of the electrodes [9]

2.3.1 Steady and Unsteady Actuation:

Thomas et al. [10] studied the effect of unsteady actuation on flow separation. Motivated by the potential decrease in the power consumption of the plasma actuator, the effect of the period of actuation on the cylinder vibration was also studied. Figure 3 shows the period of excitation in the case of unsteady actuation. For (a) and (b) the modulation frequency is the same but the duty cycle is different but for (c) the modulation frequency is twice as high. It is also worth noting that the supplied frequency (the sinusoidal frequency) is many times higher than modulation frequency.

The effect of varying the modulation frequency on the induced vibration was first investigated. It was found that plasma excitation at frequencies near the natural frequency of the cylinder (7.5 Hz) or the shedding frequency and their harmonics produce large amplitude vibrations.

Later, the modulation frequency was set at the optimum value found from the first step and the duty cycle gradually decreased to study the elimination of the vibration and the time of vibration damping as a function of the duty cycle of the modulation frequency.

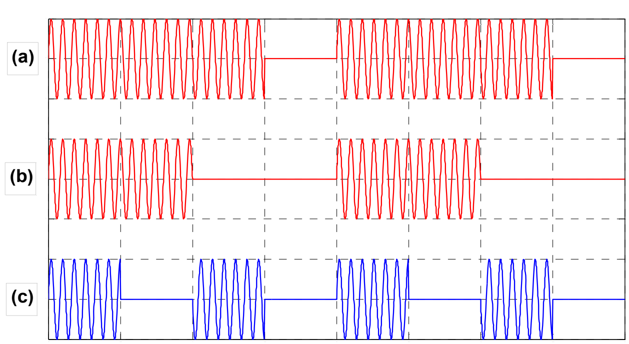

Figure 3- (a) modulation frequency (MF) = f , Duty cycle = 75% (b) MF = f , Duty cycle = 50% (c) MF = 2f , Duty cycle = 50% supplied frequency >> f

2.4 Sliding Mode Control and Stability Analysis

Sliding Mode Controller (SMC) is characterized by control laws that are discontinuous on a certain manifold in the state space, the so-called sliding surface. In SMC the state-feedback control law switches from one continuous structure to another based on the current position of the system in the state space. A SMC control law is designed such that the trajectories of the closed-loop system are attracted to the sliding surface in finite time and once on the sliding surface they slide towards the origin. By properly designing the sliding surface, SMC attains robustness regardless of parameter uncertainty and external disturbances.

Sliding mode control has long proved its capabilities. Among them, relative simplicity of design, control of independent motion (as long as sliding conditions are maintained), invariance to process dynamics characteristics and external perturbations, wide variety of operational modes such as regulation, trajectory control, and model following [12].

Due to these merits many investigators including Hossein and Baz [13,14] have studied active control of VIV using SMC. In their research Hossein and Baz have used piezo-electric actuators in conjunction with SMC to eliminate vibrations. Motivated by this work and similar research in which SMC proved its potential in VIV control, we developed SDBD-based controller.

The Sliding Mode Control scheme involves:

(I) Selection of the sliding surface such that the system trajectory exhibits desirable behavior when confined to it.

(II) Finding feedback gains so that the system trajectory intersects and stays on the manifold.

The control law in the SMC will be switched according to the distance of the state from the sliding surface.

Stability in the SMC consists of two phases: in the reaching phase the trajectory converges toward the sliding surface and in the sliding phase the trajectory stays in the surface and moves toward the origin. Figure 4 shows these two phases in phase portrait.

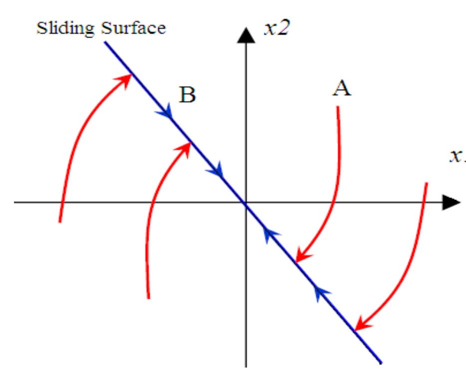

Figure 4- System trajectory
A: Reaching phase, B: Sliding Phase

It is worth indicating that in this work the plasma actuators consist of thin metal plates which are separated by thin isolating layers. Furthermore the cylinder material cannot act as a heat sink to dissipate the generated heat, so we could not operate the plasma actuator continuously. On the other hand, as discussed in the presentation of the theory of the plasma actuator, the generated force is not a continuous function of the supplied high voltage so anti-chattering algorithms based on replacing the sgn function with some continuous functions as well as saturation function cannot be applied. It was therefore necessary to develop a relay sliding mode control with hysteresis to control the position of the cylinder (vibration) and to prevent high frequency chattering as shown in Figure 5.

The body force generated by the plasma actuator was high enough to damp the vibration quickly. The actuator dynamics are many times faster than the VIV system dynamics. We could therefore ignore the delay and the nonlinearity of the actuator in order to replace the actuator model with a simple gain in the closed loop system. The level of this gain was estimated by the identification methods and by comparing the simulation and experimental results.

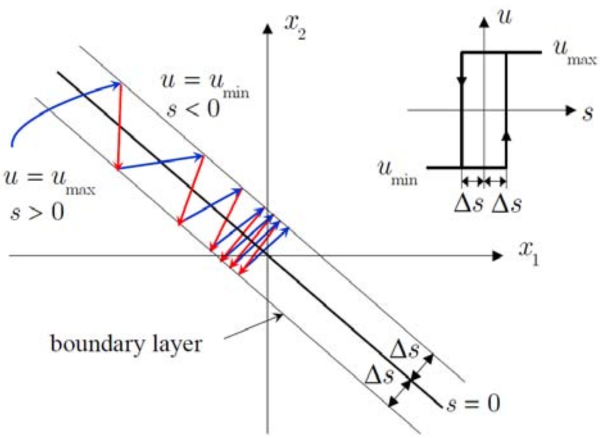

Figure 5- SMC by a relay with hysteresis
u_{min} = off acctuator and u_{max} = on acctuator

Finally two different sliding surfaces and corresponding gains were selected. The simulation and the experimental outcomes supported the design value under the worst case conditions. By rewriting the HC model in the form of state equations we have:

$$\dot{x}_1 = x_2$$
$$\dot{x}_2 = a\omega_0^2 x_3 - 2\zeta x_2 - x_1$$
$$\dot{x}_3 = x_4$$
$$\dot{x}_4 = bx_2 - \omega_0^2 x_3 - \frac{\gamma}{\omega_0} x_4^3 + \alpha\omega_0 x_4 \quad (8)$$
$$x_1 = x_r \ , \ \ x_3 = C_l$$

The sliding surfaces are:

$$S_1 = K_1 x_1 + K_2 \dot{x}_1 \quad (9)$$

$$S_2 = K_1 x_1 \quad (10)$$

In the first case to avoid the effect of the high frequency noise we used a filter as the derivative function. The control law in both cases was simply:

$$u = sgn(S_i) \quad (11)$$

Carbonell et al. [15], showed the Lyapunov stability of SMC and by using the backstepping methodology and considering suitable gains proved that SMC achieves stabilization and perfect tracking in VIV control.

3 EXPERIMENTAL APPARATUS

3.1 Wind Tunnel

The flow-control experiments were performed in a subsonic, low turbulence, recirculating wind tunnel. The wind tunnel has an inlet with contraction ratio of 20:1**,** cross section area of 60cm X 60cm, maximum velocity of 90 m/s and 0.5% turbulence intensity.

3.2 Cylinder and mounted actuators

The length and diameter of the test cylinder are respectively 29 cm and 4.1 cm. The schematic of the cylinder and mounted plasma actuators is shown in Figure 6. As indicated in the figure, the outer, exposed electrodes (3) are mounted on the surface of the cylinder with their plasma-generating edges located at 90 and 175 deg with respect to the approach flow direction. These surface electrodes are made of thick copper foil tape. The position of the electrodes comes from the idea that the best location for the pair of plasma actuators is near the separation point [18]. The actuators can be activated either in phase or out of phase. In the present work the actuators were operated in phase. This means that the resulting controlled introduces symmetrical perturbations in the flow.

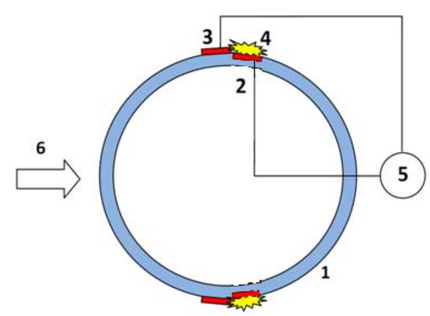

Figure 6- Cylinder and the position of actuators, the various components are : 1- Cylinder 2- Inner layer of plasma actuator 3- Outer layer of plasma actuator 4- Plasma ignition 5- High voltage power supply 6- Flow direction

3.3 High Voltage Driver

The actuator is driven by Minipulse generators. The generators are designed to generate high frequency AC voltages in the range from 5 to 30 kHz with amplitudes up to 10 kV peak (20 kVpp or 7 kV rms). The device consists of one single integrated circuit board. Power can be supplied from batteries (DC voltage) or an ordinary low DC voltage lab power unit. The generator consists of an externally controllable transistor half-bridge and a connected high voltage transformer cascade.

3.4 DAQ system and sensor

The Minipulse generator is controlled by the control algorithm and driver software developed in Labview8.0. The DAQ card used for measuring the displacement is a NI-PCI-6711 (6713 or 6715) boards with BNC-2110 (or 2120) connector. A laser sensor is utilized to measure the cylinder displacement.

4 RESULTS AND DISCUSSION

4.1 Parameter Identification

In order to generate the data needed for calculating the FIM, the HC model was simulated numerically and the algorithm presented in section 2.2 was applied to estimate the parameters covariance matrix which is given below:

Covariance Matrix =

$$\begin{bmatrix} \zeta & a & b & \gamma & \alpha \\ 2{,}7E\text{-}08 & 8{,}4E\text{-}08 & -7{,}1E\text{-}05 & -1{,}0E\text{-}06 & 3E\text{-}05 \\ 8{,}4E\text{-}08 & 9{,}5E\text{-}06 & 0{,}0018 & -0{,}0001 & -0{,}0021 \\ -7{,}1E\text{-}05 & 0{,}0017 & 0{,}6989 & -0{,}0182 & -0{,}7268 \\ -1{,}0E\text{-}06 & -0{,}0001 & -0{,}0181 & 0{,}0011 & 0{,}0225 \\ 3{,}4E\text{-}05 & -0{,}0021 & -0{,}7268 & 0{,}0225 & 1{,}1996 \end{bmatrix} \quad (12)$$

A study of the covariance matrix showed that the parameters $\boldsymbol{\zeta}$ and $\boldsymbol{a}$ can be identified accurately because their variances are negligible. The precision of $\boldsymbol{\gamma}$ is acceptable but we cannot estimate the parameters $\boldsymbol{b}$ and $\boldsymbol{\alpha}$ accurately by measuring the displacement since their variances are elevated.

Figure 7 shows the confidence ellipse between the two parameters ζ and $\boldsymbol{a}$. This type of ellipse is useful for establishing confidence intervals for the prediction of single new observations (prediction intervals). More information about confidence interval and interpretation of the confidence ellipse can be found in [16].

To identify the identifiable parameters the results of open loop experiments were used after filtering the high frequency noise. Nonlinear identification methods estimated the parameters by using the measured data as discussed below.

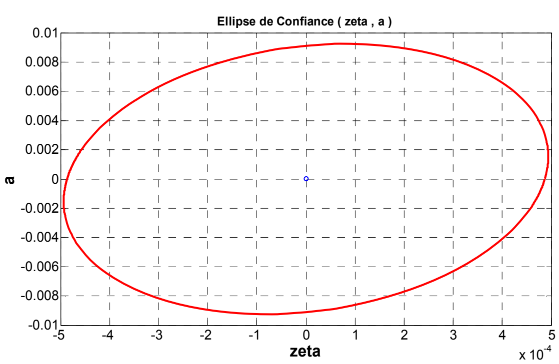

Figure 7- confidence ellipse between two parameters ζ and $\boldsymbol{a}$

The measured data is divided into two sections that can be seen in Figure 8. The first section where the vibration is increased by the vortex shedding whose frequency is near to the natural frequency of cylinder and the second section where the air flow is stopped and the vibration decreased by natural damping. In the first section a nonlinear error minimizing method was used to estimate the identifiable parameters $\boldsymbol{\zeta}, \boldsymbol{a}$ and $\boldsymbol{b}$ yielding: $\zeta = 0.0033$, $a = 0.006$ and $b = 0.39$.

In the second section by using the logarithmic decrement method [17] we calculated the natural damping factor.

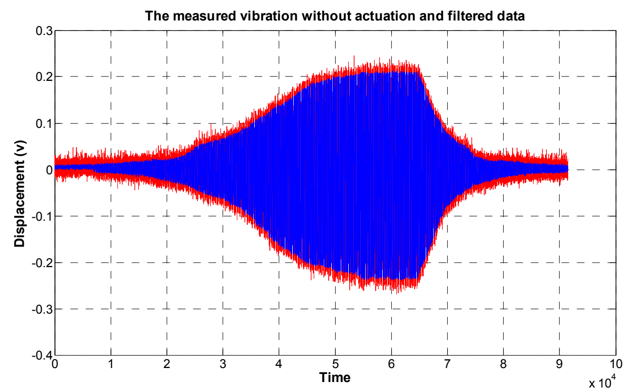

Figure 8- Measured displacement after (blue) and before (Red) filtering, without actuation

By applying this method we obtain $\zeta = 0.0032{\sim}0.0036$ **.** This value confirms the estimated value for the damping factor by the previous method.

4.2 Steady Actuation

Figure 9 shows the effect of plasma actuation on the envelop curve of the vibration. The vibration decreases dramatically toward zero in the period of actuation (A to C). The fall time in the presence of the flow and plasma actuation is about three times faster than the effect of natural damping of the cylinder. This shows that plasma actuator generate a considerable force to modify the flow and perturb the vortices.

It can be seen that the effect of plasma actuation in damping of the vibration is not uniform. The actuation period can be divided into at least two sections. In the first section (A to B) the vibration is rapidly attenuated but in the second section (B to C) when the vibration is low the slope of the curve is four or five times lower.

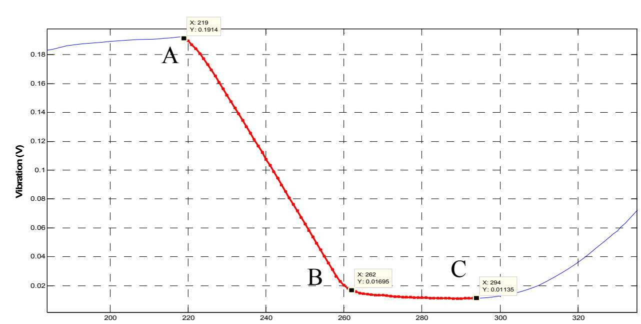

Figure 9- non-uniform effect of plasma actuation on the vibration (actuation period: Red and dotted)

This reveals a nonlinear effect of the plasma force on the vibration.

Flow visualization was accomplished by PIV imaging of the cylinder near wake. This was achieved by seeding the flow with 1 μm diam olive oil droplets. Figure 10(a,b) show the flow vorticity and velocity field without actuation. Typical Karman wake shedding is clearly visible in the near wake in Figure 10(a,b). Figure 10(c,d) presents corresponding flow visualization images with the plasma actuation operating in steady mode. This figure shows that the plasma actuation has a profound influence on the global structure of the flow, reducing the extent of the separated flow region. The Karman vortex shedding is completely eliminated as a result of plasma actuation.

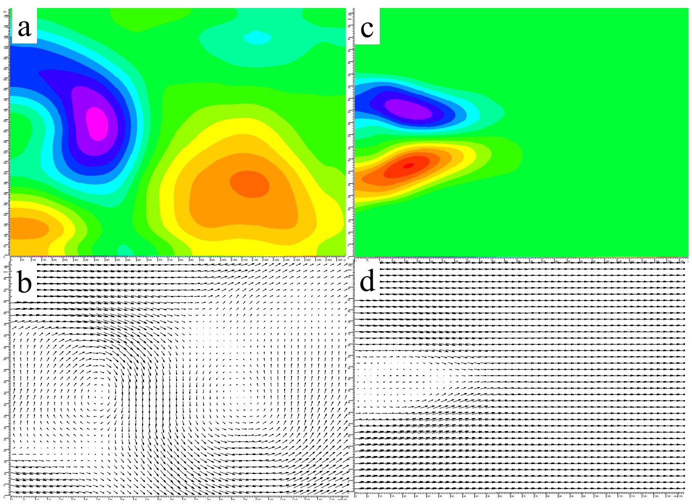

Figure 10- Laser photo of vortices
(a,b: before actuation c,d: after actuation)

4.3 Unsteady Actuation

The effect of unsteady (periodic) plasma actuation was investigated by changing the modulation frequency and duty cycle (Figure 3). Vibration measurement was used to monitor the effect of unsteady plasma actuation. It was found that optimum suppression of shedding and minimum wake defect occurred for unsteady forcing at a modulation frequency of approximately 11 Hz which is far from the natural frequency (f_n = 7.5Hz) of the cylinder and its harmonics. The modulation frequency was fixed at 11Hz and the duty cycle varied over a wide range. In each case, the plasma actuators were fired at the maximum cylinder position and the data of the vibration amplitude envelop curve was recorded for comparison. As noted earlier, the actuators are fired in phase, thus generating symmetrical perturbations in the flow. Note that symmetrical actuation here is very different from past unsteady control where normally asymmetrical actuation is often used, e.g. in [3] where cylinder rotation is used. Mureithi et al. [21] have shown that symmetrical perturbations lead to a period doubling bifurcation of the Karman wake flow. A feed forward controller based on this bifurcation was demonstrated by Mureithi et al. [22]. The controller was, however, not optimal, thus leading to the present work.

In Figure 11 the continuous decrease of actuation force and increase of the fall time due to reduction of duty cycle is obvious. With duty cycle less than 20% the vibration cannot be suppressed completely.

In this figure A to C shows the period of actuation. In the interval C to D the actuator is off. D to E shows the next period of actuation.

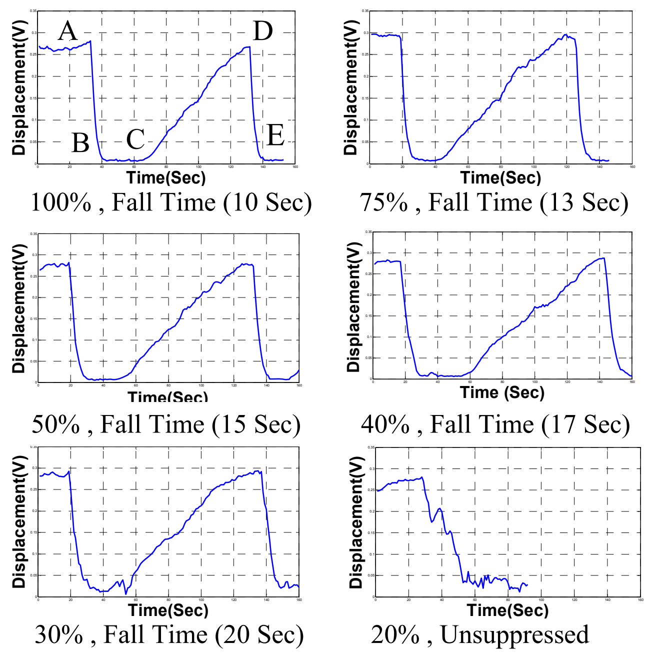

Figure 11- Vibration envelop curves for unsteady actuation with different duty cycles; modulation frequency= 11Hz

4.4 Closed loop control

Before doing any experiments, the different control algorithms were simulated in Simulink. Figure 12 demonstrates the simulation of a controller with hysteresis (the simplest form of SMC with the second sliding surface S2 (equ. 10)). As discussed above the physics of the plasma actuator and practical limitation lead us to use the actuator in the on/off mode. In order to prevent continuous chattering a hysteresis relay was added in the control algorithm loop. By adjusting this hysteresis the sensitivity of the controller and the period of plasma firing could be varied.

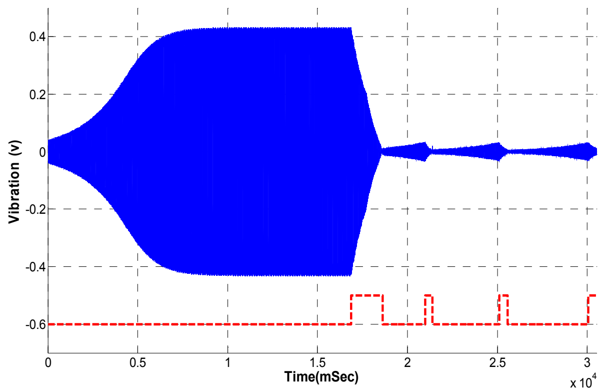

Figure 12: Simulation of the controller on the HC model Vibration (Bold), Actuation (Dashed), Hysteresis=20mv

Figure 13 and 14 show the experimental results for sliding mode controllers respectively designed for S1(9) & S2 (10). The set point and hysteresis value in these figures define the sensitivity of the controller and the threshold of the plasma firing. An envelope detector was used to measure the peak of the vibration. This signal was used as the error signal in the control algorithms to suppress the vibrations.

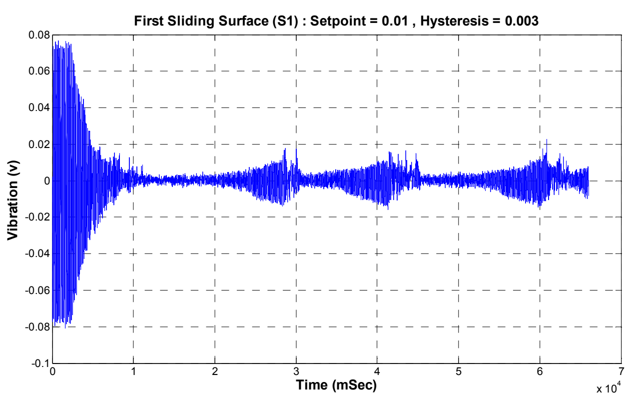

Figure 13: Experimental result of vibration control for the first form of SMC (S1) : set point=0.01 & Hysteresis=0.003

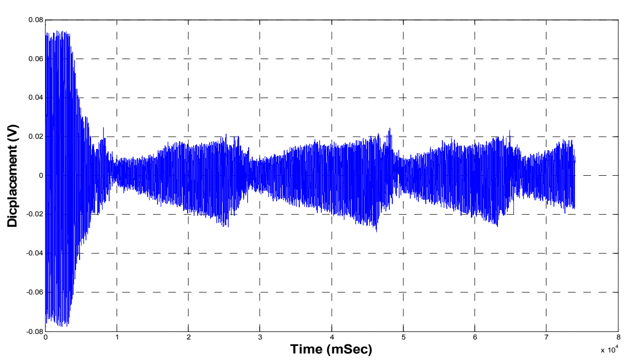

Figure 14: Experimental result of vibration control for the second form of SMC (S2): set point=0.02 & Hysteresis=0.004

Roughly speaking the effect of the derivative term in the first sliding mode surface (9) is related to the rate of vibration increase or the slope of the envelope curve. This controller can therefore predict the vibration and effectively control the displacement of the cylinder as is clear from a comparison of Figure 13 and 14.

Figure 15 and 16 demonstrate the effect of unsteady actuation in the closed loop system. The period of actuation is indicated in these figures to clearly highlight the difference. As can be seen the reduction of the duty cycle of the modulation frequency weakens the plasma force on the air and reduces its impact on the flow separation and vibration control. The control policy cannot compensate for this limitation of the actuator.

It is worth noting that by changing the geometry of the plasma actuator or by increasing the number of mounted actuators on the surface of the cylinder as well as optimizing the driving high voltage and frequency, it is possible to increase the actuator force and minimize the effective duty cycle.

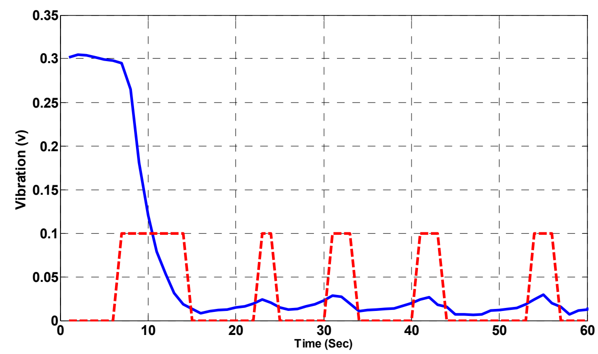

Figure 15: Envelop of vibration (Bold) and period of actuation(Dashed)
Modulation frequency=11Hz, Duty cycle =100%

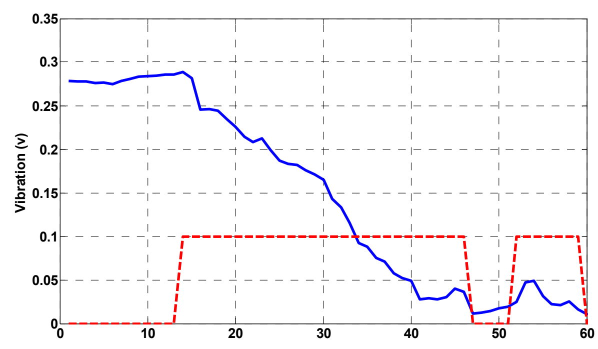

Figure 16: Envelop of vibration (Bold) and period of actuation (Dashed)
Modulation frequency=11Hz, Duty cycle =15%

5 CONCLUSION

In this paper, the identifiability of the HC model parameters by measuring the cylinder displacement was studied. Three parameters were identified accurately. The VIV of a circular cylinder was also investigated numerically and experimentally. The results of the flow-control experiments clearly demonstrate the feasibility of the plasma actuator in effectively eliminating VIV. Experiments were also carried out to investigate the suppression effect of the plasma actuation in steady and unsteady mode. Steady operation of the actuators is shown to drastically reduce the degree of flow separation and the associated Karman vortex shedding is eliminated. An associated benefit of the steady plasma actuation is minimum fall time for the vibration suppression envelop curve. It is shown that the use of unsteady plasma actuation at 30% duty cycle and a frequency far from the natural frequency and its harmonics also controls the Karman shedding and as a consequence the VIV, however, lower duty cycles approaching 15% were found to lead to reduced flow-control effectiveness.

The actuation time as a measure of consumed power showed that the power consumption can be minimized by using nonlinear control algorithms and unsteady actuation. The effectiveness of the controller in each case was investigated by studying of the damped vibration fall time.

Both our simulations and experimental results for closed loop control of VIV of the cylinder by sliding mode controllers show that the VIV of the circular cylinder can be suppressed successfully. The relay sliding mode controller proved its potential as a simple and robust method for the control of VIV in the presence of parameter uncertainty and disturbances.

REFRENCES

[1Peterka] J.A., Richardson P.D., 1969, " Effects of sound on separated flows" , Journal of Fluid Mechanics 37 (2) (1969) 265–287.

[2] Liu W.P., Brodie G.H., 2000, "A Demonstration of MEMS-Based Active Turbulence Transitioning ", International Journal of Heat and Fluid Flow
21, 297–303.

[3] Fujisawa N., Kawaji Y., Ikemoto K., 2001, "Feedback Control of Vortex Shedding from a Circular Cylinder by Rotational Oscillations", Journal of Fluids and Structures 15 , 23–37.

[4] Cheng L., Zhou Y., Zhang M.M., 2003, "Perturbed Interaction Between Vortex Shedding and Induced Vibration", Journal of Fluids and Structures 17 (7) , 887–901.

[5] Hartlen R.T.,Currie I.G., 1970, " Lift-oscillator model of vortex induced vibration", Journal of the Engineering Mechanics,96 (5) 577–591.

[6] Mureithi, N. W., Kanki, H., and Nakamura, T., 2000, ''Bifurcation and Perturbation Analysis of Some Vortex Shedding Models,'' Flow Induced Vibrations,eds., S. Ziada and T. Staubli, pp. 61–68.

[7] Mureithi N. W., Kanki, H., and Nakamura, T., 2000, ''Bifurcation and Perturbation Analysis of a Class of Vortex-Structure Interaction Models,'' Proc., International Conf. on Structural Stability and Design ~ICSSD2000.

[8] LeBeau R.P.,Reasor D.A., Suzen Y.B., 2007, "Unstructured Grid Simulations of Plasma Actuator Models", 3793, 37th AIAA Fluid Dynamics Conference.

[9] Suzen Y.B., Huang P.G., Jacob J.D., Ashpis D.E. , 2007 "Numerical Simulations of Flow Separation Control in Low-Pressure Turbines using Plasma Actuators",45th AIAA Aerospace Sciences Meeting and Exhibit, Reno NV.

[10]Thomas Flint O., Kozlov A., Corke T., 2008, "Plasma Actuators for Cylinder Flow Control and Noise Reduction" AIAA JOURNAL, Vol. 46, No. 8.

[11] Roth, J.R., Dai, X., 2006, "Optimization of the Aerodynamic Plasma Actuator as an Electro hydrodynamic (EHD) Electrical Device," 44th AIAA Aerospace Sciences Meeting and Exhibit, AIAA Paper 1203.

[12] Slotine J.J.E. and Li W., 1991,"Applied nonlinear control", Prentice Hall, ISBN 0-13-040890-5.

[13] Hussein N.,Baz A., 2008, "Active Control of Vortex-induced Vibrations using a Continuous Sliding Mode Control", AIAA 6336.

[14] Baz A., Kim M., 1993, "Active Modal Control of Vortex-induced Vibrations of a Flexible Cylinder", Journal of Sound and Vibration 165(1), 69-84.

[15] Carbonell P. Wang, X., Jiang Z., 2003, "On the suppression of flow-induced vibration with a simple control algorithm", Communications in Nonlinear Science, Vol8, P49-64.

[16] Cook R.D., 1999, "Applied Regression Including Computing and Graphics", ISBN 0-471-3171 1-X, p66

[17] Clarence W. de Silva, 2007, "Vibration Fundamentals and Practice", ISBN 0-8493-1987-0.

[18] Chen Z. Fan B., Zhou B., Li H., 2007, "Open loop control of vortex-induced vibration of a circular cylinder", Chinese Physics Soc. and IOP Publishing Ltd, Vol 16 No 4.

[19] Likhanskii A., Shneider M., Macheret S., and Miles R., 2006 , "Modeling of Interaction Between Weakly Ionized Near-Surface Plasmas and Gas Flow", *Paper AIAA-2006-1204*, 44th AIAA Aerospace Sciences Meeting and Exhibit, Reno, Nevada, Jan. 9-12

[20] Anderson, R., 2006, "Barrier Discharge Plasma Actuators for Dry and Humid Atmospheres", *Paper AIAA- 2006-0369,* 44th AIAA Aerospace Sciences Meeting and Exhibit, Reno, Nevada, Jan. 9-12

[21] Mureithi, N.W., et al., 2002, "Symmetry breaking and mode interaction in vortex-structure interaction", Paper IMECE 2002-32512, Proceedings, 5th International Symposium on FSI, AE & FIV+N, ASME Int'l Mech. Engrg. Congress & Exhibition, New Orleans, Louisiana, USA.

[22] Mureithi, N.W., M. Rodriguez, P. Versailles, A. Pham, and H.D.Vo, 2008, "A POD based analysis of the 2D cylinder wake mode interactions", Flow Induced Vibration, Zolotarev & Horacek eds.